

All-chalcogenide glass based high fill-factor long-wave infrared micro-metalens array with superior optical flexibility

Zhaofeng Gu(谷招峰), Kongsi Zhou(周孔思), Tong Sun(孙童), Yixiao Gao(高一骁), Yimin Chen(陈益敏), Zijun Liu(刘自军), Chenjie Gu(顾辰杰), Pengfei Lu(芦鹏飞), and Xiang Shen(沈祥)

Citation: Chin. Phys. B, 2025, 34 (**7**): 074213. DOI: 10.1088/1674-1056/add4f5
http://cpb.iphy.ac.cn; http://iopscience.iop.org/cpb

What follows is a list of articles you may be interested in

Third-order nonlinear wavelength conversion in chalcogenide glass waveguides towards mid-infrared photonics

Fengbo Han(韩锋博), Jiaxin Gu(顾佳新), Lu Huang(黄璐), Hang Wang(王航), Yali Huang(黄雅莉), Xuecheng Zhou(周学成), Shaoliang Yu(虞绍良), Zhengqian Luo(罗正钱), Zhipeng Dong(董志鹏), and Qingyang Du(杜清扬)
Chin. Phys. B, 2024, 33 (**10**): 104207. DOI: 10.1088/1674-1056/ad6557

Generation of mid-infrared supercontinuum by designing circular photonic crystal fiber

Ying Huang(黄颖), Hua Yang(杨华), and Yucheng Mao(毛雨澄)
Chin. Phys. B, 2022, 31 (**5**): 054211. DOI: 10.1088/1674-1056/ac272c

Ultrabroadband mid-infrared emission from Cr^{2+}:ZnSe-doped chalcogenide glasses prepared via hot uniaxial pressing and melt-quenching

Ke-Lun Xia(夏克伦), Guang Jia(贾光), Hao-Tian Gan(甘浩天), Yi-Ming Gui(桂一鸣), Xu-Sheng Zhang(张徐生), Zi-Jun Liu(刘自军), and Xiang Shen(沈祥)
Chin. Phys. B, 2021, 30 (**9**): 094208. DOI: 10.1088/1674-1056/ac11eb

Design and fabrication of GeAsSeS chalcogenide waveguides with thermal annealing

Limeng Zhang(张李萌), Jinbo Chen(陈锦波), Jierong Gu(顾杰荣), Yixiao Gao(高一骁), Xiang Shen(沈祥), Yimin Chen(陈益敏), and Tiefeng Xu(徐铁峰)
Chin. Phys. B, 2021, 30 (**3**): 034210. DOI: 10.1088/1674-1056/abd757

Experimental and numerical investigation of mid-infrared laser in Pr^{3+}-doped chalcogenide fiber

Hua Chen(陈华), Ke-Lun Xia(夏克伦), Zi-Jun Liu(刘自军), Xun-Si Wang(王训四), Xiang-Hua Zhang(章向华), Yin-Sheng Xu(许银生), Shi-Xun Dai(戴世勋)
Chin. Phys. B, 2019, 28 (**2**): 024209. DOI: 10.1088/1674-1056/28/2/024209

All-chalcogenide glass based high fill-factor long-wave infrared micro-metalens array with superior optical flexibility

Zhaofeng Gu(谷招峰)[1,2,†], Kongsi Zhou(周孔思)[1,2,†], Tong Sun(孙童)[3], Yixiao Gao(高一骁)[1,2], Yimin Chen(陈益敏)[1,2], Zijun Liu(刘自军)[1,2], Chenjie Gu(顾辰杰)[1,2,3,‡], Pengfei Lu(芦鹏飞)[3], and Xiang Shen(沈祥)[1,2,§]

[1] *Laboratory of Infrared Materials and Devices, Research Institute of Advanced Technologies, Ningbo University, Ningbo* 315211, *China*
[2] *Zhejiang Key Laboratory of Advanced Optical Functional Materials and Devices, Ningbo* 315211, *China*
[3] *Zhejiang Supermat Sen-Ray Optoelectronics Co., Ltd., Ningbo* 315400, *China*

(Received 7 February 2025; revised manuscript received 10 April 2025; accepted manuscript online 7 May 2025)

Long-wave infrared (LWIR) micro-metalens arrays have emerged as highly flexible and multifunctional optical elements, significantly enhancing the performance of infrared imaging systems. In this work, two types of chalcogenide glass based LWIR micro-metalens arrays with 10×10 array-size and 100% fill factor were designed and investigated. Specifically, the first one possesses a uniform focal length of 110 μm, and it can efficiently focus the incident light (9.78 μm) into a spot with a full width at half maximum (FWHM) of approximately 11.5 μm ($\sim 1.18\lambda$). Additionally, the second one features flexible and configurable focal lengths of the respective micro-metalenses in the array, and focal lengths of 102 μm, 149 μm, and 182 μm can be achieved on one substrate, while it still retains the same optical performance as the micro-metalens array with a single focal length. Overall, these all-chalcogenide glass based LWIR micro-metasurface arrays possess significant potential for integrating within advanced infrared imaging systems in the future.

Keywords: chalcogenide glass, multi-focal micro-metalens array, long-wave infrared, high fill factor

PACS: 42.70.−a, 42.82.Cr, 95.75.De, 78.20.Bh

DOI: 10.1088/1674-1056/add4f5 **CSTR:** 32038.14.CPB.add4f5

1. Introduction

The ongoing advancements in long-wave infrared (LWIR) sensing and imaging applications, such as wavefront sensing,[1] beam homogenizing,[2] superresolution reconstruction,[3] and gas monitoring,[4] have led to a growing demand for pixel-level optical components. In light of the aforementioned emerging essentials, LWIR microlens arrays (MLAs) comprised of arrays of micron-scale spherical lenses have been employed to effectively gather the incoming light on the LWIR focal plane array (FPA), ultimately improving the infrared imaging quality.[5,6]

Presently, the spherical lens based MLAs are fabricated by using techniques such as thermal reflow,[7] wet etching-assisted femtosecond laser direct writing,[8] ultraprecision diamond turning,[9] and molding.[10] However, it is still a huge challenge to achieve precise and uniform curvature for a large number of microlenses in the array. Recently, metasurfaces composed of two-dimensional periodic arrays of artificial micro-structures have emerged as an intriguing platform for light control.[11–15] By tuning the geometric parameters of these subwavelength optical scatterers, metasurfaces can effectively manipulate various light properties, including polarization, amplitude, and phase. Significant progress has been made in metalens technology, successfully achieving advanced optical functionalities such as wide-angle imaging[16] and chromatic aberration correction.[17] Moreover, in terms of resolution, metalenses can even outperform traditional lenses. The resolution of lenses is typically constrained by the diffraction limit, which is generally improved by increasing the numerical aperture (NA). Some reported metalenses have an NA approaching 1.[18,19] As fabrication processes continue to mature, the focus of research is gradually shifting towards large-area fabrication and array integration,[19–24] which greatly expands the practical application prospects of metalenses in complex optical systems. Metalenses offer greater flexibility in the design and fabrication of MLAs. For example, in conventional imaging systems, it is difficult to obtain the depth information from images. Although spherical artificial compound eyes can solve this problem, their fabrication and integration with FPA remain challenging.[25,26] On the other hand, flat multi-focal MLAs fabricated by using techniques like multilayer photolithography,[27] three-dimensional (3D) lithography,[28] and femtosecond laser processes[29,30] can address this issue. However, the spherical microlenses prepared by these methods face the problem of limited design flexibility, complex processes, and low efficiency.

In contrast, the principle of the metalenses eliminates the need for complex curvature control in designing parameters to

[†]These authors contributed equally to this work.
[‡]Corresponding author. E-mail: guchenjie@nbu.edu.cn
[§]Corresponding author. E-mail: shenxiang@nbu.edu.cn

© 2025 Chinese Physical Society and IOP Publishing Ltd. All rights, including for text and data mining, AI training, and similar technologies, are reserved.

achieve the desired numerical aperture and focal length. Moreover, the fabrication process of multifocal microlens arrays based on metasurface technology is compatible with semiconductor processing. The microstructures vary only in geometric dimensions and arrangement, maintaining the same height, and requiring only a single exposure and etching process, making them suitable for mass production. Furthermore, conventional commercial microlenses are typically circular, with several micrometers of spacing between each microlens. In contrast, metalens can be designed in arbitrary shapes, such as squares, and can easily achieve tight packing with a 100% filling factor, thereby enhancing light energy utilization. Additionally, relying on highly efficient and precise microfabrication techniques, the designed microstructures can be transferred to the substrate with minimal error. For example, Liu et al. demonstrated an all-silicon LWIR micro-metalens array with a uniform focal length, which can efficiently focus a CO_2 laser beam with a wavelength of 10.6 μm with a focusing efficiency of $\sim 34\%$.[31] At this stage, it is worth mentioning that, although silicon material offers reliable manufacturing capabilities, it exhibits significant absorption beyond 7 μm,[32] limiting its performance in the LWIR range. However, other low-loss LWIR materials, such as some fluorides (CaF_2 and BaF_2), have low refractive indices. To achieve 2π phase coverage, high aspect ratio microstructure designs are required, which are challenging to fabricate. Therefore, ZnS and ZnSe are the most popular optical materials in the LWIR range, with low absorption and moderate refractive indices. However, these materials suffer from slow etching rates, making them unsuitable for fabricating microstructures with micron-level heights in the LWIR range. Germanium (Ge) exhibits low absorption losses and a high refractive index in the LWIR range. Wang *et al.*[33] fabricated a mid-infrared metalens using germanium. However, the high refractive index of germanium also leads to significant reflection losses, requiring additional antireflection coatings to mitigate this problem.[34] Furthermore, germanium has a large refractive index temperature coefficient ($\mathrm{d}n/\mathrm{d}T$) of 396×10^{-6} K^{-1},[35] which causes the shift of the focal length due to environmental temperature variations, thereby affecting image quality.

Chalcogenide glass (ChG) is an amorphous material composed of chalcogen elements (sulfur, selenium, or tellurium), which offers numerous advantages.[36] For example, it has high refractive index, wide infrared transmission range, low absorption losses, and low $\mathrm{d}n/\mathrm{d}T$, making it an ideal material for the fabrication of LWIR micro-metalens arrays.[37] Among them, As_2Se_3 glass is an excellent commercially available chalcogenide glass material, and we compare its performance with the materials mentioned earlier (see Table S3).

In this paper, we present the design and fabrication of two types of 10×10 transmissive and polarization-independent LWIR micro-metalens arrays based on chalcogenide glass. The first one possesses a uniform focal length and the other one is designed to have multi-focal lengths on a single substrate. Each micro-metalens in the array is square-shaped with 100% fill factor. Using the 9.78-μm laser as the light source, the uniform-focal micro-metalens array can focus the incident light into a spot with a full width at half maximum (FWHM) of approximately 11.5 μm ($\sim 1.18\lambda$) at the focal plane. The multi-focal micro-metalens array, featuring focal lengths of 102 μm, 149 μm, and 182 μm, can focus the incident light to the specific focal plane with the same optical performance as obtained on the micro-metalens array with a single focal length. It is believed that these all-chalcogenide glass-based micro-metalens arrays will have significant potential for applications in compact thermal imaging systems.

2. Experiment and equipment

The designed micro-metalens array was fabricated through electron beam lithography (EBL) patterning and inductively coupled plasma (ICP) etching. The EBL system (Raith eLINE Plus, Germany) was employed to write the negative pattern of the micro-metalens array. Subsequently, hard metals were deposited by sputtering (Lesker PVD 75, USA) and lifted-off to create a mask with a positive pattern. ICP (Oxford Instruments, PlasmaPro 100 Cobra, UK) was then used to etch the micro-metalens array. Scanning electron microscope (SEM) images of the micro-metalens array morphology were also obtained using the EBL system. The light at the focal point was collected through a reflective objective (ROL, Thorlabs, LMM-40X-P01) and directed to an infrared FPA (IRay Technology Co., Ltd., M3640, China) to obtain the focal spot image. The light source was a quantum cascade laser (QCL, Ningbo Healthy Photon Co., Ltd., China), emitting collimated LWIR light at 9.78 μm. For imaging tests, the "N", "B", and "U" letter patterns were irradiated by a blackbody reference source (CEM, BX-500, China).

3. The micro-metalens array with uniform focus

In this section, we first analyze the refractive index and transmittance curves of As_2Se_3 glass in the LWIR range (Fig. S1). The refractive index of As_2Se_3 glass at a wavelength of 9.78 μm is measured to be 2.781, with minimal variation in refractive index over the 8–12 μm wavelength range, exhibiting low dispersion characteristics. Furthermore, in this wavelength range, the transmittance reaches up to $\sim 63\%$ with no noticeable absorption peaks, indicating its extremely low-loss properties. We then present the design process of the all-chalcogenide glass material based micro-metalens array with the same focus. First, a simple and effective local phase modulation unit cell is employed, which consists of numbers

of cylindrical As_2Se_3 micropillars with varying diameters arranged in a square lattice. Due to the symmetry of the in-plane cross-section of the micropillars, the propagation phase is independent of the polarization of the incident light. When incident light impinges on the unit cell, each As_2Se_3 micropillar can be regarded as a truncated micro-waveguide. The electromagnetic field shows that the light field is tightly confined in the micropillars, and the inter-pillar coupling effect can be neglected (Fig. S2). Figure 1(a) shows a schematic of the unit cell, where the height and diameter of the micropillar are denoted by H and D, and the period is denoted by P. Finite-difference time-domain (FDTD) simulations are used to calculate the corresponding transmission and phase shift curves for the micropillars (Fig. 1(b)). The diameters of the pillars range from 2.0 μm to 4.8 μm, where $P = 5.5$ μm and $H = 8$ μm. It should be emphasized that the average transmission is mainly determined by the refractive index of the substrate. Therefore, compared to LWIR metalenses based on silicon and germanium, the lower refractive index of As_2Se_3 contributes to a higher average transmission due to reduced reflection losses. The phase shift can be expressed as $\varphi = k_0 n_{\text{eff}} H$, where n_{eff} is the effective refractive index, and variations in n_{eff} lead to phase shift modulation.[38] From this equation, it can be known that larger micropillar diameters induce greater phase shifts in the transmitted light. Therefore, eight micropillars with different diameters are selected as the design units for the micro-metalens. These micropillars introduce linear phase delays from 0 to $7\pi/4$, incremented by $\pi/4$. We also know that the height H of the dielectric micropillars also influences the phase shift. When the height of the micropillar is 8 μm, it is suitable for achieving 2π phase coverage. By spatially arranging micropillars with varying phase shift capabilities, the wavefront can be efficiently controlled.

A single micro-metalens can transform a plane wavefront into a converging wavefront (Fig. 1(c)). The phase profile $\varphi(x,y)$ of the micro-metalens under normal incident light can be described by a radially symmetric phase shift function

$$\varphi(x,y) = \frac{2\pi}{\lambda}(f - \sqrt{x^2+y^2+f^2}). \tag{1}$$

Here, x and y represent the Cartesian coordinates, with the origin located at the center of the micro-metalens, φ denotes the phase shift at position (x,y), λ is the working wavelength in free space, and f represents the designed focal length. According to the phase shift function, where the focal length f is set to 110 μm, eight micropillars with different diameters are arranged in a discontinuous manner to meet the discrete phase distribution of the single micro-metalens, as shown in Fig. 1(d). To achieve a 100% fill factor in the micro-metalens array, the micro-metalenses are designed with a square shape, each with a side length of 115.5 μm. We then performed simulations of the focusing characteristics of the designed micro-metalens array using the FDTD method. For efficiency, a 3×3 micro-metalens array was used in the simulations to reduce the size of the 3D simulation domain. Figure 1(e) shows the normalized field intensity distribution along the x–z plane at $y = 0$ μm, where incident light is tightly focused near $z = 110$ μm, consistent with the design. Figure 1(f) shows the normalized field intensity distribution at the focal plane (in the x–y plane), with the FWHM of the focal spot along the y direction of 8.7 μm. A good focusing effect of the micro-metalens array can be observed, with no noticeable crosstalk between adjacent micro-metalenses. Finally, the designed single micro-metalens is used as the second basic unit element to form a 10×10 micro-metalens array for fabrication. Compared to traditional infrared bulk lenses, which focus by accumulating propagation phases of curved surface, this metasurface-based micro-metalens offers advantages such as flatness, thinness, design flexibility, and simple fabrication.

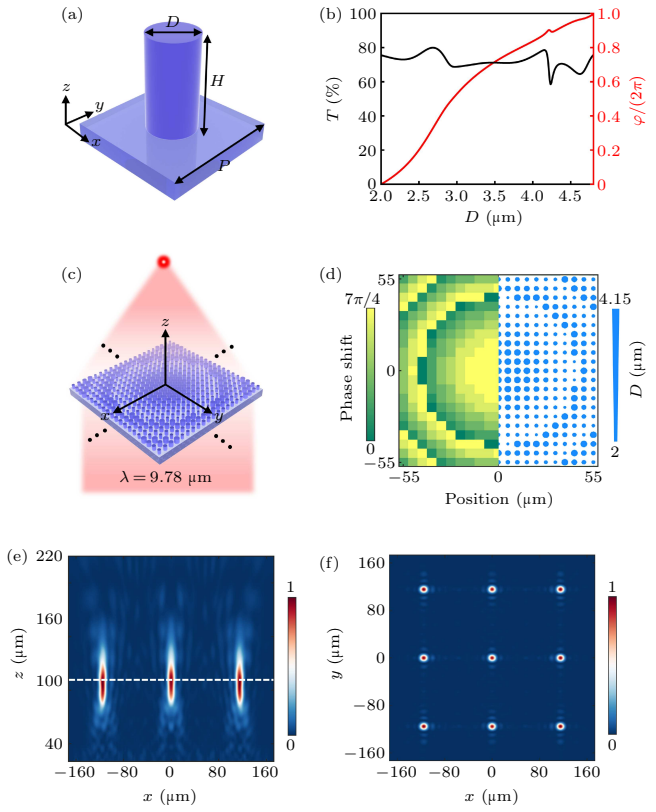


Fig. 1. (a) Schematic of a polarization-independent metasurface unit cell. Both the micropillars and the substrate are made of As_2Se_3 glass. (b) The transmission intensity T and phase shift φ of the incident light with a free-space wavelength $\lambda = 9.78$ μm as a function of the micropillar diameter D. (c) Schematic of light focusing by a single micro-metalens under vertically incident plane-wave illumination. (d) Design of an individual micro-metalens. (e) Simulated normalized field intensity distribution on the x–z plane at $y = 0$ μm. (f) Normalized field intensity distribution in the x–y plane at the focal plane $z = 110$ μm in panel (e).

Figure 2(a) illustrates the fabrication process of the micro-metalens array device. The chalcogenide glass is first cut and polished to ensure parallelism and smoothness on both sides before being used in subsequent processing steps. It

should be noted that since the smallest diameter of our micropillars is 2 μm, it is suitable for ultraviolet (UV) lithography, which facilitates large-area and high-efficiency manufacturing. Here, we use EBL for a simple demonstration, avoiding the need for custom masks. First, a positive electron beam resist layer and a conductive resist are spin-coated on the glass substrate. The pattern for the negative micro-metalens array is then generated through EBL. Subsequently, aluminum (Al) with a thickness of 30 nm and chromium (Cr) with a thickness of 60 nm are successively deposited onto the patterned photoresist film, followed by a lift-off process to remove the resist, leaving only the positive pattern on the substrate. The As_2Se_3 glass with the metal hard mask is then etched away by using a mixture of CHF_3 and CF_4 plasma in an ICP system. Although chalcogenide glasses are considered soft in terms of mechanical properties, we successfully fabricated micropillars with a height of 8 μm and a maximum aspect ratio of 4:1 using an optimized deep etching process. Finally, the residual metal mask is removed by using hydrochloric acid, completing the fabrication of the micro-metalens array. Figure 2(b) displays a representative SEM image of the fabricated As_2Se_3 micro-metalens array with uniform focal length, showing good morphology and 100% fill factor. Figure 2(c) presents an SEM image of the fabricated micro-metalens array taken at an inclined angle, revealing that the sidewalls of the micropillars are nearly vertical.

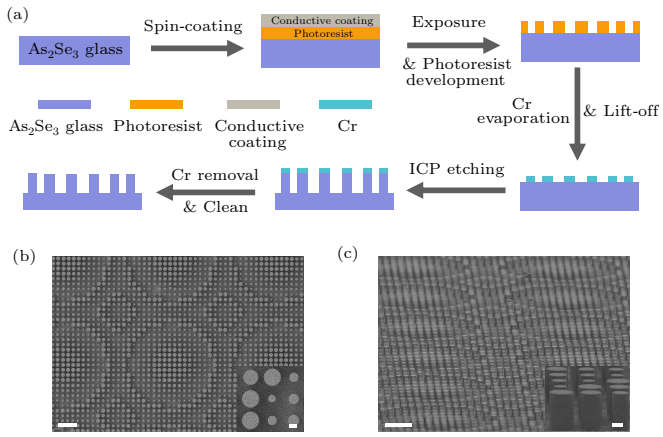


Fig. 2. (a) Process flow for fabricating the micro-metalens array. (b) and (c) SEM images of the fabricated micro-metalens array with uniform focal length at different tilt angles. The scale bars in (b) and (c) are 20 μm, and all insets show magnified views with scale bars of 2 μm.

To evaluate the performance of the fabricated micro-metalens array, we conducted focusing and thermal imaging tests. Figure 3(a) shows a schematic of the measurement setup. A quantum cascade laser emits a collimated beam with a wavelength of 9.78 μm, which is directed through the back of an unstructured substrate to irradiate the micro-metalens array. The transmitted light is collected by a reflecting objective lens and then guided to an LWIR focal plane array for imaging the focused spots. The resolution of the focal plane array is 640×512 with a pixel size of 12 μm × 12 μm. Both the FPA and ROL are mounted on a translation stage (Newport, M-462-XYZ-M). Figure 3(b) shows the focal spot image of the fabricated micro-metalens array with a focal length of approximately 110 μm. Figure 3(c) shows the experimental and simulated normalized intensity distributions along the *y*-axis cross-section. The measured actual FWHM at the focus is approximately 11.5 μm ($\sim 1.18\lambda$), which is slightly larger than the simulated value of 8.7 μm.

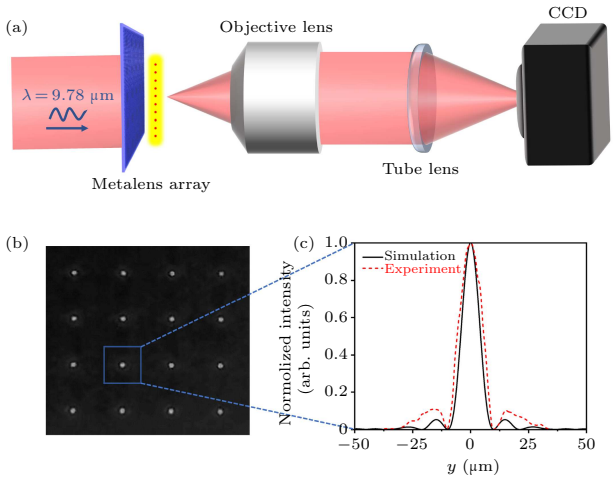


Fig. 3. (a) The test setup used to characterize the focusing performance of the fabricated micro-metalens array. (b) Spot image taken at the focal plane. (c) A cross-sectional plot of the simulated intensity distribution (black line) and the measured intensity distribution (red dashed line) along the *y*-axis at the focal plane.

To further evaluate the imaging performance, we used the fabricated uniform-focal micro-metalens array to image the polymer-printed hollow letter patterns "N", "B", and "U" with the high-temperature blackbody as the thermal source. The results showed that each micro-metalens in the array was able to produce relatively clear images of the letters "N", "B", and "U", further confirming the reliability of the fabricated uniform-focal micro-metalens array. It should be noted that due to chromatic aberration, the broadband thermal emission from the high-temperature blackbody source caused slight blurring at the edges of the letters. The chromatic aberration that occurs when imaging with a metalens under broadband light sources arises from factors such as material dispersion and the strong wavelength dependence of the phase modulation characteristics. These factors lead to different degrees of displacement of different wavelengths of light on the focal plane. This wavelength-dependent chromatic aberration degrades image quality, manifesting as edge halos and blurring. To eliminate this chromatic aberration, designing chromatic metalenses can effectively address the aberration at different wavelengths, thereby reducing halo effects and enabling broadband light source imaging. In recent years, chromatic metalenses designed using methods such as group delay or plasmonic resonance have been reported,[17,39–41] achieving

phase matching across multiple wavelengths, ensuring that light focuses onto the same focal plane over a broad wavelength range. Additionally, a composite structure, such as a hybrid metalens doublet incorporating a refractive lens and a metasurface corrector, can also achieve chromatic aberration and astigmatism correction across a broad wavelength range.[42] Moreover, it should be noted that the slight differences in imaging clarity of these metalenses may be attributed to the following factors: small angular deviations in the micro-metalens array sample, inhomogeneity of the blackbody light source, or defects and contamination occurring during the manufacturing process. Adjusting the sample angle to ensure perpendicular light incidence, using a more uniform light source, and optimizing the fabrication process of the microlens array (including improving the consistency of overall microstructure height, ensuring vertical sidewall angles, and enhancing cleanliness) could improve the uniformity of the microlens array in imaging tests.

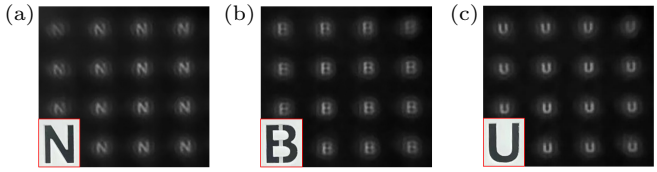


Fig. 4. Images of the hollow letter logos (a) "N", (b) "B", and (c) "U" under high temperature blackbody illumination, captured by the fabricated uniform-focal micro-metalens array.

4. The micro-metalens array with multiple focuses

The principle of light manipulation of the metalens offers greater flexibility and convenience in optical parameter design. Unlike the conventional spherical microlenses, which rely on complex surface profiles to control wavefronts, micro-metalenses modulate the wavefront by introducing abrupt phase shifts. The focal length of multi-focal MLAs is no longer dependent on the simultaneous control of the curvature of multiple distinct surface profiles. Instead, it is determined by a different arrangement of subwavelength microstructural units coming from the same library and having the same height. This approach significantly simplifies the design and fabrication process. In the subsequent experiment, different focal lengths of the micro-metalenses are achieved by re-selecting and arranging the existing microstructure unit library according to the phase shift function (Eq. (1)). We then designed and fabricated a 10×10 multi-focal micro-metalens array with three different focal lengths: $f_1 = 102$ μm, $f_2 = 149$ μm, and $f_3 = 182$ μm, with each square micro-metalens having a size of 115.5 μm × 115.5 μm. The focusing schematic of the multi-focal micro-metalens is shown in Fig. 5(a), the micro-metalens can focus incident light at three different depths, thereby extending the depth of field. Figure 5(b) shows the simulated normalized field intensity distribution along the x–z plane for a 3×3 multi-focal micro-metalens array. Incident light is focused near $f_1 = 102$ μm, $f_2 = 149$ μm, and $f_3 = 182$ μm, confirming the validity of the design.

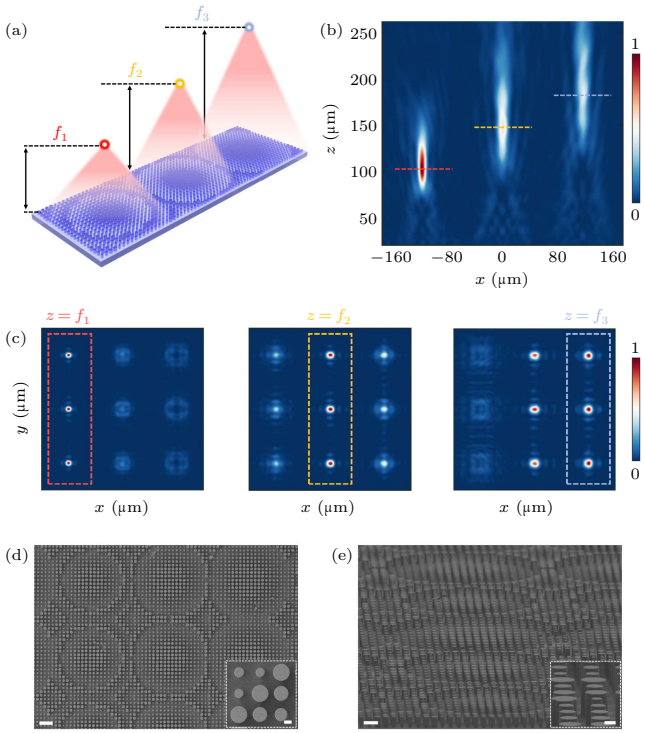


Fig. 5. (a) Schematic of multi-focus micro-metalens array. (b) Normalized intensity distribution in the x–z plane after passing through the 3×3 multi-focal micro-metalens array in the simulation. (c) Simulated intensity distribution in the x–y plane for $z = f_1$, f_2, and f_3. (d) and (e) SEM images of the fabricated multi-focal micro-metalens array at different tilt angles, with scale bars of 20 μm and 10 μm, respectively. All insets are magnified images, with scale bars of 2 μm.

Additionally, the impact of crosstalk between metalenses in the array on the focal length was analyzed through simulations (Fig. S3). The focusing efficiencies of the f_1, f_2, and f_3 metalenses are 48%, 53%, and 55%, respectively. It can be observed that as the focal length increases, the numerical aperture decreases, leading to a reduction in focusing performance. However, the focusing efficiency improves. This can be attributed to the fact that as the focal length increases, the FWHM of the metalens also increases, resulting in a greater light field energy within the calculated spot. The focusing efficiency is defined as the ratio of the optical field energy within a circular region, determined by three times the FWHM, at the focal plane to the total incident optical energy on the metalens. The intensity distribution of light spots at different focal planes along the z-axis in the simulation is shown in Fig. 5(c). The multi-focal micro-metalens array follows the same fabrication process, and SEM images of the fabricated sample are shown in Figs. 5(d) and 5(e), where the morphology of the microstructures also has good verticality. The arrangement of

micropillars within each micro-metalens varies according to the different focal lengths in the multi-focal micro-metalens array.

We performed imaging tests on the fabricated multi-focal micro-metalens array, which provides a more intuitive demonstration of its unique optical performance. Figure 6(a) illustrates the imaging principle for different focal lengths, where the magnification of the imaging pattern depends on the focal length of the micro-metalenses with the same aperture size. A high-temperature soldering iron was used as a broadband LWIR source, and Fig. 6(b) shows a photo of the soldering iron. Figures 6(c)–6(e) present the captured images of the high-temperature soldering iron through the fabricated multi-focal micro-metalens array, demonstrating its ability to focus at three different depths. The circles correspond to the imaging effects of the three micro-metalenses with focal lengths of $f_1 = 102$ μm, $f_2 = 149$ μm, and $f_3 = 182$ μm, respectively. It can be observed that good imaging performance is obtained when focusing at three different image planes, with varying magnifications due to their different focal lengths. With a constant object distance, the micro-metalens with a larger focal length forms an image that is both farther and larger. Similarly, due to chromatic aberration, the broadband thermal emission of the high-temperature soldering iron also causes slight blurring at the edges of the image.

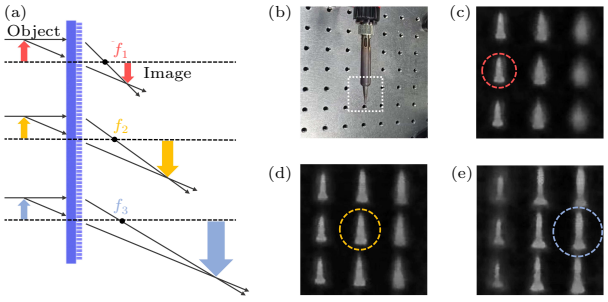


Fig. 6. (a) Schematic of the imaging principle of multi-focal micro-metalens array with different focal lengths, showing that the magnification of the image depends on the focal length of micro-metalens with the same aperture. (b) Photo of the soldering iron. (c)–(e) Images of the soldering iron captured by multi-focal micro-metalens array with focal lengths $f_1 = 102$ μm, $f_2 = 149$ μm, and $f_3 = 182$ μm.

5. Conclusion

In summary, we have theoretically and experimentally demonstrated an LWIR uniform-focal and multi-focal micro-metalens array based on chalcogenide glass. Each micro-metalens is square-shaped with a 100% fill factor and consists of micropillars with varying diameters, which achieve high transmittance while covering a phase shift range from 0 to 2π. The fabricated uniform-focal micro-metalens array can effectively focus LWIR light, with the FWHM of the focal spot approximately 1.18λ. Additionally, we fabricated a multi-focal micro-metalens array with flexible phase designs and verified its multi-focal imaging performance. Due to its lightweight, easy integration, design flexibility, and simple fabrication, the metasurface-based micro-metalens array has become an effective alternative to conventional MLAs. We believe these metasurface-based, all-chalcogenide glass LWIR micro-metalens arrays offer significant potential for next-generation, multifunctional, efficient, and compact thermal imaging systems.

Acknowledgments

Project supported by the Natural Science Foundation of Zhejiang Province (Grant Nos. LDT23F05015F05 and LDT23F05011F05) and the Joint Funds of the National Natural Science Foundation of China (Grant No. U24A20313).

References

[1] Velghe S, Primot J, Guérineau N, Haïdar R, Demoustier S, Cohen M and Wattellier B 2006 *Proc. SPIE* **6292** 62920
[2] Holmes A S, Bich A, Meunier M, Rieck J, Dumouchel C, Arnold C B, Niino H, Roth S, Weible K J, Geohegan D B, Träger F, Eisner M, Voelkel R, Dubowski J J, Zimmermann M, Rank M, Schmidt M, Bitterli R, Ramanan N, Ruffieux P, Scharf T, Noell W, Herzig H P and De Rooij N 2008 *Proc. SPIE* **6879** 68790Q
[3] Shankar M, Willett R, Pitsianis N, Schulz T, Gibbons R, Kolste T, Carriere J C, Chen D P and Brady D 2008 *Appl. Optics* **47** B1
[4] Xu H, Xu L, Zhu W and Zhang L 2024 *Appl. Optics* **63** 5515
[5] Rogalski A 2003 *Prog. Quant. Electron.* **27** 59
[6] Luo Z, Hou H, Meng T, Li Y, Wang T, Yi Y, Xu L, Chen Z, Zhong H, Feng Y, Zhang P and Zhao Y 2024 *ACS Photonics* **11** 4597
[7] Shi J, Huang Y S, Peng L N, Ni Z J and Zhang D W 2020 *Opt. Mater.* **104** 109733
[8] Zhou W, Li R, Li M, Tao P, Wang X, Dai S, Song B, Zhang W, Lin C, shen X, Xu T and Zhang P 2022 *Ceram. Int.* **48** 18983
[9] Mukaida M and Yan J 2017 *Int. J. Mach. Tool. Manu.* **115** 2
[10] Zhou T, Liu X, Liang Z, Liu Y, Xie J and Wang X 2017 *Front. Mech. Eng-PRC.* **12** 46
[11] Arbabi A, Horie Y, Bagheri M and Faraon A 2015 *Nat. Nanotechnol.* **10** 937
[12] Kamali S M, Arbabi E, Arbabi A and Faraon A 2018 *Nanophotonics* **7** 1041
[13] Fan Q, Liu M, Yang C, Yu L, Yan F and Xu T 2018 *Appl. Phys. Lett.* **113** 201104
[14] Luo X 2018 *Adv. Opt. Mater.* **6** 1701201
[15] Tseng M L, Hsiao H H, Chu C H, Chen M K, Sun G, Liu A Q and Tsai D P 2018 *Adv. Opt. Mater.* **6** 1800554
[16] Zhang N, Li Q, Chen J, Tang F, Wu J, Ye X and Yang L 2022 *Chin. Phys. B* **31** 074212
[17] Wang S, Wu P C, Su V C, Lai Y C, Chen M K, Kuo H Y, Chen B H, Chen Y H, Huang T T and Wang J H 2018 *Nat. Nanotechnol.* **13** 227
[18] Paniagua-Dominguez R, Yu Y F, Khaidarov E, Choi S, Leong V, Bakker R M, Liang X, Fu Y H, Valuckas V and Krivitsky L A 2018 *Nano Lett.* **18** 2124
[19] Fan Z B, Shao Z K, Xie M Y, Pang X N, Ruan W S, Zhao F L, Chen Y J, Yu S Y and Dong J W 2018 *Phys. Rev. Appl.* **10** 014005
[20] Fan Z B, Qiu H Y, Zhang H L, Pang X N, Zhou L D, Liu L, Ren H, Wang Q H and Dong J W 2019 *Light Sci. Appl.* **8** 67
[21] Fan Z B, Cheng Y F, Chen Z M, Liu X, Lu W L, Li S H, Jiang S J, Qin Z and Dong J W 2024 *eLight* **4** 3
[22] Park J S, Lim S W D, Amirzhan A, Kang H, Karrfalt K, Kim D, Leger J, Urbas A, Ossiander M and Li Z 2024 *ACS Nano* **18** 3187
[23] Lim S W D, Meretska M L and Capasso F 2021 *Nano Lett.* **21** 8642
[24] Park J S, Zhang S, She A, Chen W T, Lin P, Yousef K M, Cheng J X and Capasso F 2019 *Nano Lett.* **19** 8673
[25] Luan S, Cao H, Deng H, Zheng G, Song Y and Gui C 2022 *ACS Appl. Mater. Interfaces* **14** 46112
[26] Phan H, Yi J, Bae J, Ko H, Lee S, Cho D, Seo J M and Koo K I 2021 *Micromachines* **12** 847

[27] Bae S I, Kim K, Yang S, Jang K W and Jeong K H 2020 *Opt. Express* **28** 9082
[28] Cao H, Deng H, Wan H, Luan S, Shen S and Gui C 2023 *ACS Omega* **8** 48572
[29] Yan M, Li R, Li M, Liu S, Zhou G, Lin C, Dai S, Song B, Zhang W, Xu T and Zhang P 2024 *Opt. Laser Technol.* **174** 110601
[30] Chen Z, Yuan H, Wu P, Zhang W, Juodkazis S, Huang H and Cao X 2021 *Opt. Lett.* **47** 22
[31] Liu M, Fan Q, Yu L and Xu T 2019 *Opt. Express* **27** 10738
[32] Soref R A, Emelett S J and Buchwald W R 2006 *J. Opt. A-Pure. Appl. Op.* **8** 840
[33] Wang A, Chen Z and Dan Y 2019 *AIP Adv.* **9** 085327
[34] Nalbant H C, Balli F, Yelboga T, Eren A and Sozak A 2022 *Appl. Optics* **61** 9946
[35] Icenogle H W, Platt B C and Wolfe W L 1976 *Appl. Optics* **15** 2348
[36] Han F, Gu J, Huang L, Wang H, Huang Y, Zhou X, Yu S, Luo Z, Dong Z and Du Q 2024 *Chin. Phys. B* **33** 104207
[37] Gu Z, Gao Y, Zhou K, Ge J, Xu C, Xu L, Rahmani M, Jiang R, Chen Y and Liu Z 2024 *Opto-Electron. Sci.* **3** 240017
[38] Khorasaninejad M, Zhu A Y, Roques-Carmes C, Chen W T, Oh J, Mishra I, Devlin R C and Capasso F 2016 *Nano Lett.* **16** 7229
[39] Arbabi E, Arbabi A, Kamali S M, Horie Y and Faraon A 2017 *Optica* **4** 625
[40] Wang S, Wu P C, Su V C, Lai Y C, Hung Chu C, Chen J W, Lu S H, Chen J, Xu B and Kuan C H 2017 *Nat. Commun.* **8** 187
[41] Chen W T, Zhu A Y, Sanjeev V, Khorasaninejad M, Shi Z, Lee E and Capasso F 2018 *Nat. Nanotechnol.* **13** 220
[42] Liu M, Zhao W, Wang Y, Huo P, Zhang H, Lu Y Q and Xu T 2024 *Nano Lett.* **24** 7609